scientific reports

Check for updates

OPEN

Development of a tissue-engineered oral mucosal barrier model using poly (L-lactic acid) electrospun nanofibers

Andari Sarasati[1], Deniz Yucel[2,4], Halime Kenar[3,4], Hevi Wihadmadyatami[5,6], Neval Sevinc Ozdemir[2,7,8], Rahmi Anggraeni[6,9], Vasif Hasirci[3,4,10] & Ika Dewi Ana[6,11,12,13]✉

The oral mucosa is a crucial barrier that defends against external factors and regulates tissue permeability. To advance trans-epithelial drug delivery and dental biomaterials research, a robust in vitro model of oral mucosal tissue is needed. This study develops an oral epithelial model using electrospun poly (L-lactic acid) (PLA) meshes. Two PLA formulations (10% and 12% in $CHCl_3$/ DMF) were optimized for nanoscale fibers production and subsequently functionalized via O_2 plasma treatment and fibronectin coating to enhance cell adhesion by increasing surface hydrophilicity, as measured by contact angle analysis. Oral epithelial cells (TR146) were cultured on these scaffolds. Adhesion and proliferation were evaluated using confocal microscopy and both MTS and PrestoBlue viability assays. The 12% PLA formulation produced fibers with an average diameter of 717 nm and pore sizes of approximately 366 nm, significantly improving cell adhesion and proliferation. Functionalization further enhanced cell attachment and spreading through increased hydrophilicity and targeted protein interactions. Confocal imaging revealed uniform cell distribution and multilayered growth that mimics native oral epithelium architecture. These findings demonstrate that fibronectin-coated 12% PLA electrospun meshes are promising scaffolds for oral epithelial tissue engineering and trans-epithelial delivery applications.

Keywords Poly (L-lactic acid), Electrospun nanofibrous mesh, Cell behaviour, Oral mucosal barrier, Tissue engineering

The World Health Organization (WHO) estimates that nearly 50% of the global population suffers from oral mucosal diseases[1]. The oral mucosa functions as a complex barrier, defending the body against physical, chemical, and microbiological challenges while regulating tissue permeability. It employs morphological, physiological, and biochemical defence mechanisms[2]. Structurally, the oral mucosa comprises three tissue layers. Those are a stratified squamous epithelium, a basement membrane, and the lamina propria, which together control the passage of molecules and mediate communication between the external environment and internal tissues. The outer epithelial layers play a primary role in regulating permeability, as the basement membrane and lamina

[1]Doctoral Study Program, Faculty of Dentistry, Universitas Gadjah Mada, Yogyakarta 55281, Indonesia. [2]Department of Histology and Embryology, School of Medicine, Acibadem University, Istanbul 34758, Turkey. [3]Department of Biomedical Engineering, Faculty of Engineering Sciences, Acibadem University, Istanbul 34758, Turkey. [4]Acibadem University Biomaterials A&R Center, Istanbul 34758, Atasehir, Turkey. [5]Department of Anatomy, Faculty of Veterinary Medicine, Universitas Gadjah Mada, Yogyakarta 55281, Indonesia. [6]Research Collaboration Center for Biomedical Scaffolds, National Research and Innovation Agency (BRIN) and Universitas Gadjah Mada (UGM), Bulaksumur 55281, Yogyakarta, Indonesia. [7]Department of Pharmaceutical Basic Sciences, School of Pharmacy, Acibadem University, Istanbul 34758, Turkey. [8]Department of Medical Biotechnology, ACU Graduate School of Health Sciences, Istanbul 34758, Turkey. [9]Research Center of Preclinical and Clinical Medicine, Cibinong Science Center, National Research & Innovation Agency of the Republic of Indonesia, Bogor 16915, Indonesia. [10]BIOMATEN, METU Center of Excellence in Biomaterials and Tissue Engineering, Ankara 06800, Turkey. [11]Department of Dental Biomedical Science, Faculty of Dentistry, Universitas Gadjah Mada, Yogyakarta 55281, Indonesia. [12]Center of Excellence for Carbonate Apatite-based Extracellular Matrix and Adjuvant, Universitas Gadjah Mada, Yogyakarta 55281, Indonesia. [13]Department of Dental Biomedical Sciences, Faculty of Dentistry, Universitas Gadjah Mada, Jalan Denta 1, Sekip Utara, Bulaksumur, Yogyakarta 55281, Indonesia. ✉email: ikadewiana@ugm.ac.id

propria are comparatively more permeable[3]. Disruptions or alterations in these barriers can precipitate oral pathologies and systemic diseases[4].

Moreover, the oral cavity displays significant morphological and physiological diversity[5,6]. It contains both keratinizing (e.g., buccal and sublingual tissues) and non-keratinizing epithelia (e.g., palatal and gingival tissues), with non-keratinized regions offering greater permeability due to the absence of water-impermeable acyl ceramides and the keratin layer[7]. This attribute facilitates trans-epithelial drug delivery via paracellular, i.e., tight junction-regulated, involving proteins such as occludins linked to actin via zonula occludens[8] and intercellular pathways, though these barriers may be compromised during inflammation or infection[9].

Buccal and sublingual mucosa are particularly promising for non-invasive drug delivery due to their lower enzymatic activity and high vascularization, which enhances systemic bioavailability and avoids the hepatic first-pass effect[10,11]. However, challenges remain in optimizing pharmaceutical formulations for trans-buccal delivery because of the complexity of oral biological factors. A major limitation is the absence of a standardized model for the buccal route. Existing ex vivo and in vivo models often fail to replicate human epithelial physiology accurately, and the use of animal models raises ethical concerns[12]. Advances in tissue engineering now offer in vitro alternatives using cell lines and scaffold-based 2D or 3D models to emulate oral mucosal architecture[11]. Among various approaches, electrospun nanofibers have attracted considerable attention for their ability to mimic the extracellular matrix (ECM) and provide a supportive microenvironment for cell adhesion, growth, and intercellular communication[13]. This biomimetic nanofiber meshes serve as excellent platforms for studying epithelial behaviour, the formation of tight junctions, and overall tissue organization[14].

Meanwhile, poly (L- lactic acid) (PLA) is a leading candidate for electrospinning applications due to its biocompatibility and biodegradability. However, unmodified PLA lacks sufficient cell adhesion properties, which can be improved through surface functionalization with ECM proteins[15]. This study aims to develop an in vitro model of oral mucosa using buccal epithelial cells cultured on functionalized electrospun PLA meshes. Such a model is essential for advancing dental research in areas including the development of dental materials, oral drug delivery systems, mucosal vaccinations, and innovative mouthwashes.

Materials and methods

Preparation of electrospun nanofibrous mesh

Pre-determined concentration of PLA solutions were prepared for nanofiber fabrication. Preliminary optimization experiments were conducted to determine an appropriate PLA concentration for electrospinning. PLA solutions covering a broader concentration range were initially evaluated by varying solution concentration and electrospinning parameters to assess fiber continuity, bead formation, and overall scaffold morphology. Based on these preliminary trials and previous studies using the same material system, PLA concentrations of 10% and 12% (w/v) were identified as the most suitable for producing uniform, bead-free fibers with sufficient mechanical stability for subsequent surface modification and cell culture experiments. Lower concentrations resulted in unstable jet formation and bead defects, whereas higher concentrations produced overly dense and thick fibers that were less favorable for cellular interaction. Consequently, 10% and 12% PLA were selected for further optimization and characterization.

First, PLA granules were dissolved in chloroform ($CHCl_3$) and stirred overnight to ensure homogeneity. Next, dimethylformamide (DMF) was added to achieve the desired $CHCl_3$/DMF solvent ratio, and the solution was thoroughly mixed prior to electrospinning. Electrospinning was then conducted using the parameters detailed in Table 1 to produce uniform, bead-free fibers. A 10 mL syringe fitted with an open-ended, blunt stainless-steel needle was used to load the solution, and each sample was deposited over a 30-minute period. The fibers were collected on aluminum foils pre-coated with 5% PEG (807488, Sigma-Aldrich). The entire process was maintained at 22–23 °C and 25–27% humidity. Finally, the electrospun fibers were dried in a fume hood for 24 h before further use.

Characterization of electrospun nanofibrous mesh

Scanning electron microscopy (SEM) was used to evaluate the surface morphology, fiber diameter, and porosity of the nanofibrous meshes. Samples were sputter-coated with a thin gold layer under vacuum using a Leica EM ACE600 sputter coater prior to imaging. SEM imaging was performed on a Zeiss Evo 10 SEM at an accelerating voltage of 5 kV with magnifications of 2000x and 5000x. Image analysis was carried out using ImageJ software, with measurements obtained from 100 randomly selected fibers and pores per sample across the full image area, representing technical replicates for morphological characterization. Histograms were generated to illustrate the size distributions. The thickness of the nanofibrous meshes was measured using a Digital Outside Micrometre (Model 3109–25 A, Insize) with a range of 0–25 mm, with 10 measurements taken per sample with three biological replicates to ensure accuracy.

Water contact angle measurements were performed using a Drop Shape Analyzer (DSA100, Kruss) at room temperature. To create a flat surface, the meshes were secured on a custom insert made from an Eppendorf tube. A 5 µL water droplet was carefully deposited on each sample, and contact angle measurements were performed

PLA concentration (weight%)	Solvent ratio ($CHCl_3$/DMF)	Voltage (kV)	Flow rate (mL/h)	Working distance (cm)
12	75:25	18	0.6	25
10	90:10	15	0.3	25

Table 1. Electrospinning parameters for PLA solutions.

using three biological replicates, with three technical measurements per sample. The results were analysed to determine the average contact angle and standard deviation.

Cell culture

This study employed TR146 cells (10032305, ECACC) as a model for buccal epithelial cells to simulate the buccal mucosal tissue barrier. The cells were cultured in T75 flasks using HAMS F12 medium (01-095-1 A, Sartorius), supplemented with 10% foetal bovine serum (F7524, Sigma-Aldrich), penicillin-streptomycin (10,000 U/mL), and amphotericin B. The medium was refreshed every 2–3 days, and cells were passaged with 0.25% Trypsin-EDTA (25200056, Gibco™) when they reached 80–90% confluency. Cells between passages $P+15$ and $P+20$ were used for the experiments.

Indirect cytotoxicity assay

Using indirect exposure MTS cell viability assays assessed potential toxicity from residual organic solvents. Samples were prepared in triplicate and secured with Cell Crown™ (Z681881, Sigma Aldrich) in a 24-well plate, then submerged in 1.5 mL of cell culture medium for 24 h to produce mesh extracts. TR146 cells (2×10^4 per well) were seeded in 96-well plates and allowed to adhere for 24 h before the culture medium was replaced with the mesh extracts. Cells were then incubated for 1, 3, or 7 days.

Approximately 20 µL of MTS reagent (ab197010, Abcam) was added to each well, followed by a 4-hour incubation in a CO_2 incubator. Absorbance was measured at 490 nm using a VICTOR® Nivo™ Multimode Plate Reader (PerkinElmer). Wells with untreated cells served as negative controls, while 20% DMSO in the culture medium was used as a positive control for cytotoxicity. Cellular viability was determined by comparing the absorbance of the experimental wells with that of the negative control and performed with three technical replicates per sample. The data were presented as the mean absorbance and cellular viability percentage along with their standard deviations.

Functionalization of nanofibrous mesh and cell seeding conditions

The nanofibrous electrospun meshes were immobilized into CellCrown™ inserts (Z681881) with a defined inner surface area of 0.79 cm^2. Two distinct treatments were employed: one group underwent O_2 plasma treatment, and the other was coated with fibronectin. For the plasma treatment, the meshes were exposed to O_2 plasma using a Diener Plasma Pico at 30 W for one minute. In contrast, the fibronectin group was treated with a 50 µg/mL solution of human plasma fibronectin (33016-015, Gibco™); this solution was applied onto the mesh surface, incubated at 37 °C for one hour, and then allowed to dry completely under a biosafety cabinet.

Prior to cell seeding, all samples were disinfected by UV exposure and treated with absolute ethanol for 30 min on each side. Untreated meshes served as the negative control. Approximately 100,000 cells (1.2×10^5 cells per cm^2) were seeded onto each mesh, and the medium was refreshed every two days. Confocal imaging with phalloidin-DAPI staining was performed to evaluate and establish the optimal treatment for enhancing cell adhesion and spreading.

Determination of cellular proliferation

For each experiment, three meshes were immobilized in a CellCrown insert within a 24-well plate. Next, 500 µL of a TR146 cell suspension (10^5 cells per mesh) was applied to the apical side of the fiber mesh, while 1 mL of culture medium was added to the basolateral compartment. Cellular viability and proliferation were measured using PrestoBlue (A13261, Invitrogen) at 1-, 3-, 7-, and 14-days post-seeding. Prior to the assay, the meshes were washed and the medium was replaced for a PrestoBlue working solution (diluted 1:10 with culture medium). After incubating for 2 h at 37 °C in a 5% CO_2 environment, 100 µL aliquots of the supernatant were transferred in triplicate to 96-well plates for analysis. Wells containing the PrestoBlue solution without cells served as negative controls. Absorbance readings were taken at 570 nm, using 600 nm as the reference wavelength, on a VICTOR® Nivo™ Multimode Plate Reader (PerkinElmer). The resulting data were analysed to calculate the average absorbance and the percentage of PrestoBlue reduction.

Cell staining

Cell morphology and distribution on the mesh were observed by staining the F-actin and nuclei of the cells. The seeded cells on nanofibrous PLA were fixed with 4% paraformaldehyde for 30 min at room temperature. The samples were washed with PBS 3 times prior to permeabilization with 0.1% Triton X-100 for 15 min at room temperature. After being washed, the samples were incubated in a blocking buffer consisting of 3% bovine serum albumin (BSA) for 30 min at room temperature. Flash Phalloidin™ Green 488 (424201, Biolegend) and ZO-1 (Invitrogen) was used for staining (1:100) and incubated for 1 h at room temperature. Nuclei were counterstained with a 1:1000 DAPI solution for 10 min. Confocal imaging was subsequently performed using a Zeiss CLSM 900 to visualize and assess cell distribution and morphology on the mesh.

Statistical analysis

All data are presented as mean ± standard deviation (SD) from triplicate analyses unless otherwise stated. Prior to statistical analysis, data normality was assessed using the Shapiro–Wilk test, and homogeneity of variances was evaluated using Levene's test. Statistical analyses were performed using GraphPad Prism 9. Comparisons among multiple groups were conducted using one-way analysis of variance (ANOVA) followed by Tukey's multiple comparison post hoc test. A p value < 0.05 was considered statistically significant.

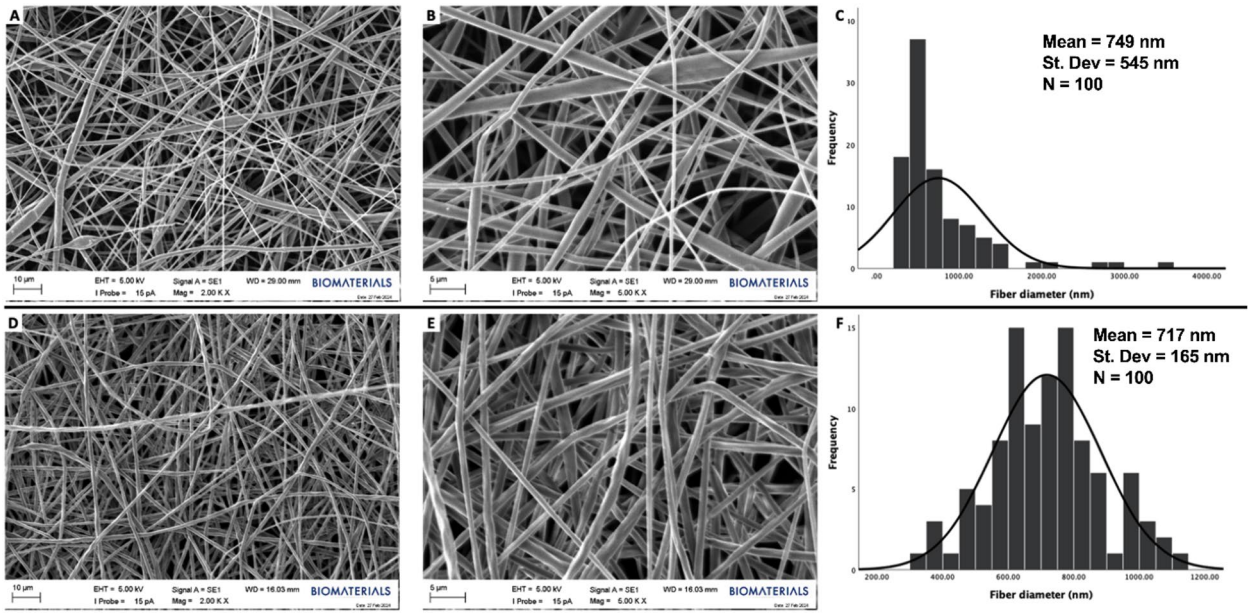

Fig. 1. Electrospun PLA fibers produced from 10% solutions (**A** and **B**) and 12% solutions (**D** and **E**), along with their corresponding diameter distributions for 10% PLA (**C**) and 12% PLA (**F**). The results show that the 12% PLA scaffolds exhibit a tighter and more uniform fiber diameter distribution compared with the 10% PLA samples (n=100).

Sample	Average fiber diameter (nm)	Maximum fiber diameter (nm)	Minimum fiber diameter (nm)	Mesh thickness (µm)
10% PLA	749 ± 545	3582	202	16 ± 3
12% PLA	717 ± 165	1104	343	16 ± 5

Table 2. Characteristics of PLA fibers diameter size and mesh thickness.

Sample	Pore number	Total area (µm)	Average size (µm)	Feret's diameter (µm)	Min Feret (µm)	Aspect ratio	% area	Circularity (%)	Solidity (%)
10% PLA	1307	925.68	0.708	1.183 ± 0.983	0.633 ± 0.530	1.87	7.28	0.755	0.843
12% PLA	660	241.53	0.366	0.817 ± 0.796	0.432 ± 0.409	1.89	1.92	0.777	0.854

Table 3. Pore characteristics of PLA electrospun meshes.

Results

Characterization of PLA nanofibrous mesh

To assess the surface morphology and fiber diameters of electrospun PLA meshes prepared from 10% to 12% solutions scanning electron microscopy (SEM) was employed. The 10% PLA scaffolds (Fig. 1A **and B**) exhibited a highly variable distribution of fiber diameters with numerous elongated beads, whereas the 12% PLA meshes displayed a notably more uniform structure. Using ImageJ, diameters were measured on 100 random fibers. The resulting distributions are illustrated in Fig. 1C **and F**.

On average, fibers (n = 100) from the 10% PLA samples measured 749 ± 545 nm, while those from the 12% PLA averaged 717 ± 165 nm. Furthermore, the 10% PLA fibers demonstrated a substantially broader range (up to 3379 nm, with a maximum diameter of 3582 nm), in contrast to the 12% PLA fibers, which peaked at 1104 nm (Table 2). Shapiro–Wilk tests indicate that the 12% PLA data conformed to a normal distribution with a narrow range (approximately 760 nm). Notably, the 12% PLA data conformed to a normal distribution with a narrow range (approximately 760 nm). Measurements of the overall mesh thickness revealed no significant differences between the two formulations.

A detailed pore size analysis was conducted on both scaffold types using ImageJ (Table 3). The 10% PLA meshes displayed a more open fiber network, resulting in larger and more abundant pores compared to the denser 12% PLA samples. Quantitatively, the 10% meshes had a total pore area of 925.68 µm^2, corresponding to 7.28% of the overall area, whereas the 12% samples exhibited a markedly lower total pore area of 241.53 µm^2. The average pore dimension measured 708 nm for the 10% PLA, significantly exceeding the 366 nm observed for the 12% formulation. Furthermore, Feret's diameter analysis indicated that the maximum pore size for 10% PLA was 1.183 µm compared to 0.817 µm for 12% PLA, while the minimum pore dimensions were 0.633 µm

and 0.432 µm, respectively. Both sample types possessed elongated pores, as indicated by their aspect ratios; however, circularity metrics revealed that the pores in the 10% PLA scaffolds were slightly less circular and more elongated. Additionally, solidity values suggested that pores in the 10% PLA were less compact, with a lower average solidity than those observed in the 12% PLA samples. The PLA concentration and solvent ratio were optimized to obtain a homogeneous, smaller fiber diameter, and smaller pore size to enable better cellular behaviour without penetration passing through the electrospun mesh, thus 12% with a 75:25 ($CHCl_3$/DMF) solvent ratio were chosen for further analysis and experiments.

Wettability of functionalized PLA nanofibrous mesh

To improve cell adhesion and subsequent cellular behaviour, electrospun PLA scaffolds were modified via two surface functionalization techniques. They were O_2 plasma treatment and fibronectin coating (Fig. 2). Unmodified PLA exhibited substantial hydrophobicity, with a water contact angle of $127 \pm 9°$. Exposure to O_2 plasma treatment resulted in only a slight reduction, achieving a contact angle of $125 \pm 2°$. In contrast, the fibronectin-coated scaffolds demonstrated a significant decline in hydrophobicity, with the water contact angle decreasing to $110 \pm 17°$ ($p < 0.05$), thereby enhancing the surface's potential for cellular interaction.

Cytotoxicity of PLA nanofibrous mesh

Cytotoxicity of the nanofibrous PLA scaffold was assessed to evaluate any adverse effects from the material or residual solvents. An indirect assay was conducted by incubating the scaffolds in cell culture medium for 24 h to generate extracts, which were then applied to cells over a seven-day period. The MTS assay, employing 20% DMSO as a positive control, revealed that cell viability consistently exceeded 85% on days 1, 3, and 7, surpassing the standard 70% viability threshold for biomedical devices. Additionally, TR146 cells cultured with the PLA

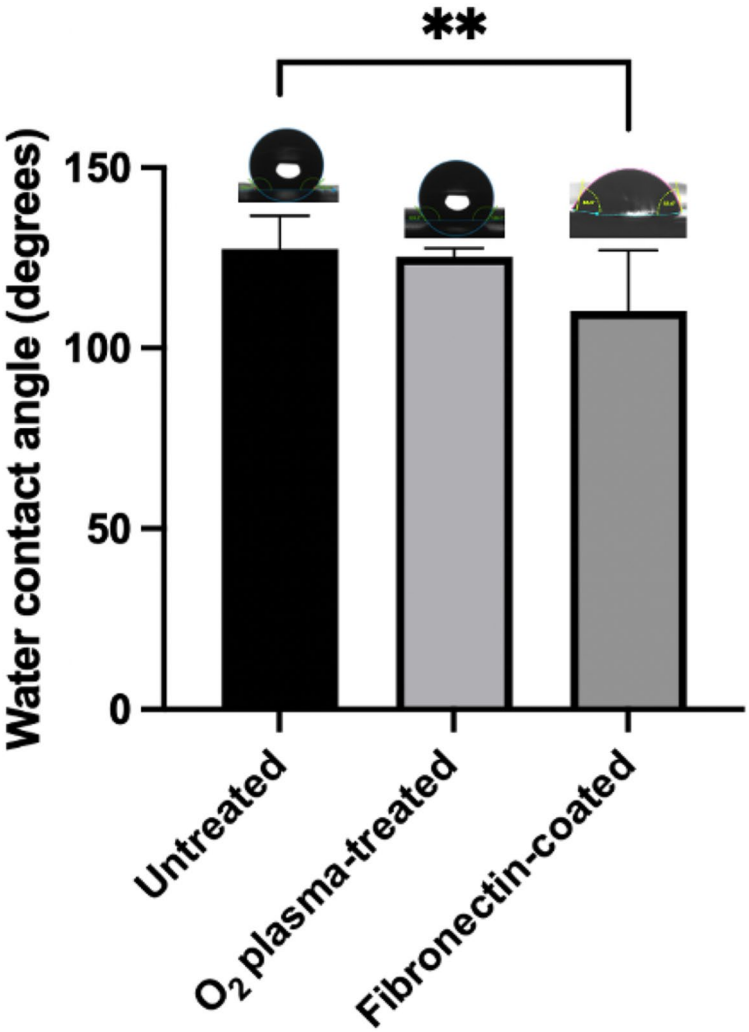

Fig. 2. Wettability of 12% PLA nanofibrous sheets in untreated, O_2 plasma–treated, and fibronectin-coated conditions. The results indicate reduced hydrophobicity in the fibronectin-coated samples (n=3), with measurements were performed in triplicate per sample.

mesh extract demonstrated progressive proliferation, as indicated by a gradual increase in absorbance over time (Fig. 3B).

Effects of PLA concentrations to cellular adhesion

Untreated PLA scaffolds were used to compare how differing polymer concentrations influence TR146 cell adhesion and spreading. After 48 h of culture, cells were stained with phalloidin and DAPI to visualize F-actin and nuclei, respectively (Fig. 4). Phalloidin imaging revealed the organization of the cytoskeleton and confirmed the epithelial morphology of the cells. Notably, the 12% PLA scaffold (Fig. 4D) exhibited a more homogeneous and complete cell coverage with well-organized actin networks, whereas the 10% PLA scaffold (Fig. 4A) showed less dense coverage and more sporadic cell clustering. Meanwhile, DAPI staining further demonstrated that 12% PLA supports a more uniform distribution of nuclei (Fig. 4E) compared to the grouped clusters observed in 10% PLA (Fig. 4B). These findings suggest that the 12% PLA scaffold provides a more favourable environment for cell attachment and proliferation. Although some gaps were evident on the 12% PLA surface, they were considerably less frequent than those observed in the 10% PLA samples.

Effects of mesh surface treatment to cell adhesion

Surface functionalization of 12% PLA electrospun scaffolds was implemented to enhance their surface properties and promote optimal cell adhesion and function. Two modification strategies, i.e., oxygen plasma treatment and fibronectin coating, were applied. The scaffolds were then seeded with cells for 48 h. After incubation, the samples were stained with phalloidin and DAPI, followed by confocal laser scanning microscopy examination.

The unmodified 12% PLA, serving as a control, exhibited sparse cell adhesion, with cells clustering irregularly across the surface (Fig. 5A **to C**). In contrast, oxygen plasma treatment yielded a more uniform cell layer, characterized by fewer voids and a higher density of cell nuclei, indicative of increased proliferation (Fig. 5D **to F**). The fibronectin-coated scaffolds produced the most favourable outcomes, with cells evenly populating the entire surface and displaying well-defined cytoskeletal arrangements (Fig. 5G **to I**). These findings suggest that fibronectin functionalization significantly improves cell attachment and distribution, creating an optimal environment for cell growth and tissue development.

Cell proliferation

A PrestoBlue assay was conducted on fibronectin-coated 12% PLA nanofibrous scaffolds to evaluate cell viability and proliferation over time. Measurements were taken on days 1, 3, 7, and 14. The absorbance readings steadily increased throughout the 14-day period (Fig. 6A), indicating robust cellular proliferation. In addition, cellular metabolic activity exhibited a significant elevation, particularly between days 3 and 7 (Fig. 6B), indicating sustained cell growth and active metabolism on the scaffold.

Actin organization

High-magnification imaging revealed detailed insights into the morphology and actin cytoskeletal organization of TR146 cells on the electrospun mesh (Fig. 7). The cells exhibited extensive spreading and formed tight, uniformly distributed networks on the substrate. Their classical epithelial features were evident, with densely stained, round nuclei, and well-organized actin filaments demonstrate robust attachment, proliferation, and confluency. The actin cytoskeleton formed a consistent, mesh-like network throughout the cell body, with clearly defined linear bundles, as an indication of stress fiber formation, arranged in parallel and intersecting patterns. These structures are hallmarks of strong cell–matrix interactions. Notably, these attributes were most pronounced in fibronectin-coated 12% PLA meshes, where enhanced peripheral fluorescence highlighted a well-developed cortical actin layer essential for maintaining cell shape and facilitating effective cell–cell interactions.

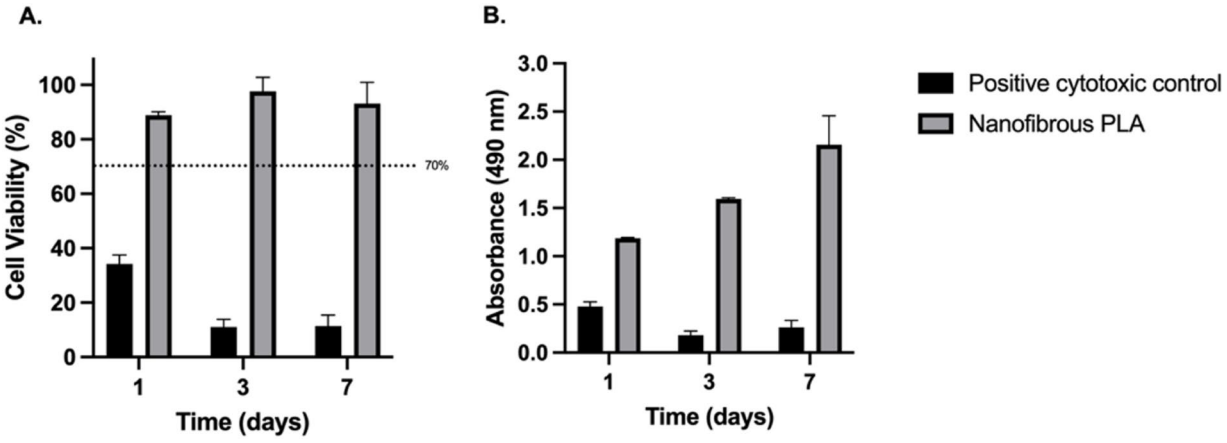

Fig. 3. Indirect cytotoxicity testing of TR146 cells exposed to nanofibrous PLA mesh extracts using MTS assays on days 1, 3, and 7 shows (**A**) cell viability and (**B**) absorbance. The exposure of TR146 cells to the nanofibrous PLA mesh extracts indicates high cell viability and sustained proliferative activity over time. Measurements were performed in triplicate.

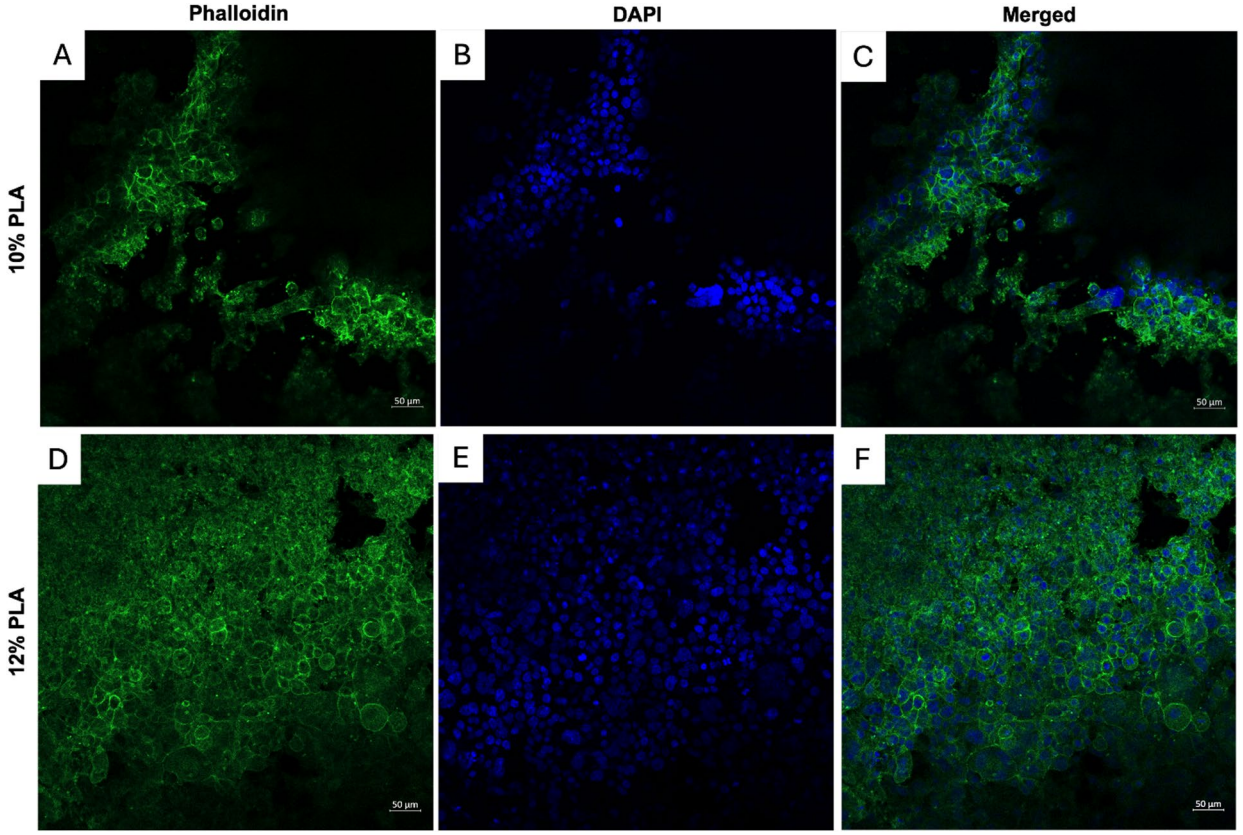

Fig. 4. The CLSM images show TR146 cells seeded on 10% PLA (**A**–**C**) and 12% PLA (**D**–**F**). Actin filaments were stained with phalloidin (green) on day 2, and cell nuclei were counterstained with DAPI (blue). Scale bar: 50 µm.

Layers of TR146 cells on PLA nanofibrous mesh

Z-stack images from orthogonal sections were captured to evaluate the three-dimensional cell distribution on the electrospun PLA meshes at days 2, 7, and 14 (Fig. 8). These images reveal that cells are broadly distributed across the scaffold, with clearly defined actin networks and nuclei throughout each plane. Vertical extensions of actin filaments across multiple focal layers confirm the formation of multilayered cell structures, supporting substantive cytoskeletal organization and cell–cell connectivity. Although nuclei are present in all layers, some regions exhibit higher cellular density than others, as seen in both X–Z and Y–Z views, which confirms a uniform vertical arrangement.

At day 2, the cell layers displayed an uneven thickness, averaging 17.01 ± 1.82 µm and forming a double-layer structure (Fig. 8A **to C**). By day 7, the overall thickness increased modestly and became more uniform, with cells appearing more densely packed rather than forming additional distinct layers. By day 14, the cell layer thickness reached 29.97 ± 2.46 µm, indicating the formation of approximately three layers (Fig. 8G **to I**). Although some areas on day 14 exhibited darker regions in the phalloidin images (suggestive of cell indentation or variations in actin filament density), the corresponding DAPI staining confirmed nuclei were present, ruling out the formation of cell-free zones. In contrast, examination of the tight junction–associated protein ZO-1 after 14 days revealed weak and discontinuous staining, without clearly defined junctional localization between adjacent cells (Fig. 9C).

Discussions

This study aimed to construct an in vitro oral epithelial tissue model for advancing trans-epithelial delivery research. Electrospun poly (lactic acid) (PLA) served as a surrogate basement membrane due to its tuneable structure and ability to mimic the extracellular matrix (ECM), a critical factor for promoting cell function and interaction[16]. The adjustable fiber diameter and extensive surface area of electrospun PLA provided an effective platform that supports cell adhesion and proliferation, which are essential in tissue engineering applications[17].

The cellular response to the fibers was notably affected by their physical, chemical, and mechanical properties. Previous research has indicated that nanoscale fibers, especially those with reduced diameters, can significantly influence cell behaviour[18]. In this study, two poly(lactic acid) (PLA) formulations were optimized to produce nanoscale fibers. Both formulations enabled cell attachment; however, the 12% PLA variant demonstrated superior cell adhesion. Confocal microscopy of the 10% PLA scaffolds revealed uneven cell distribution with prominent clustering (Fig. 4A), a phenomenon likely related to inconsistent fiber diameters, bead formation,

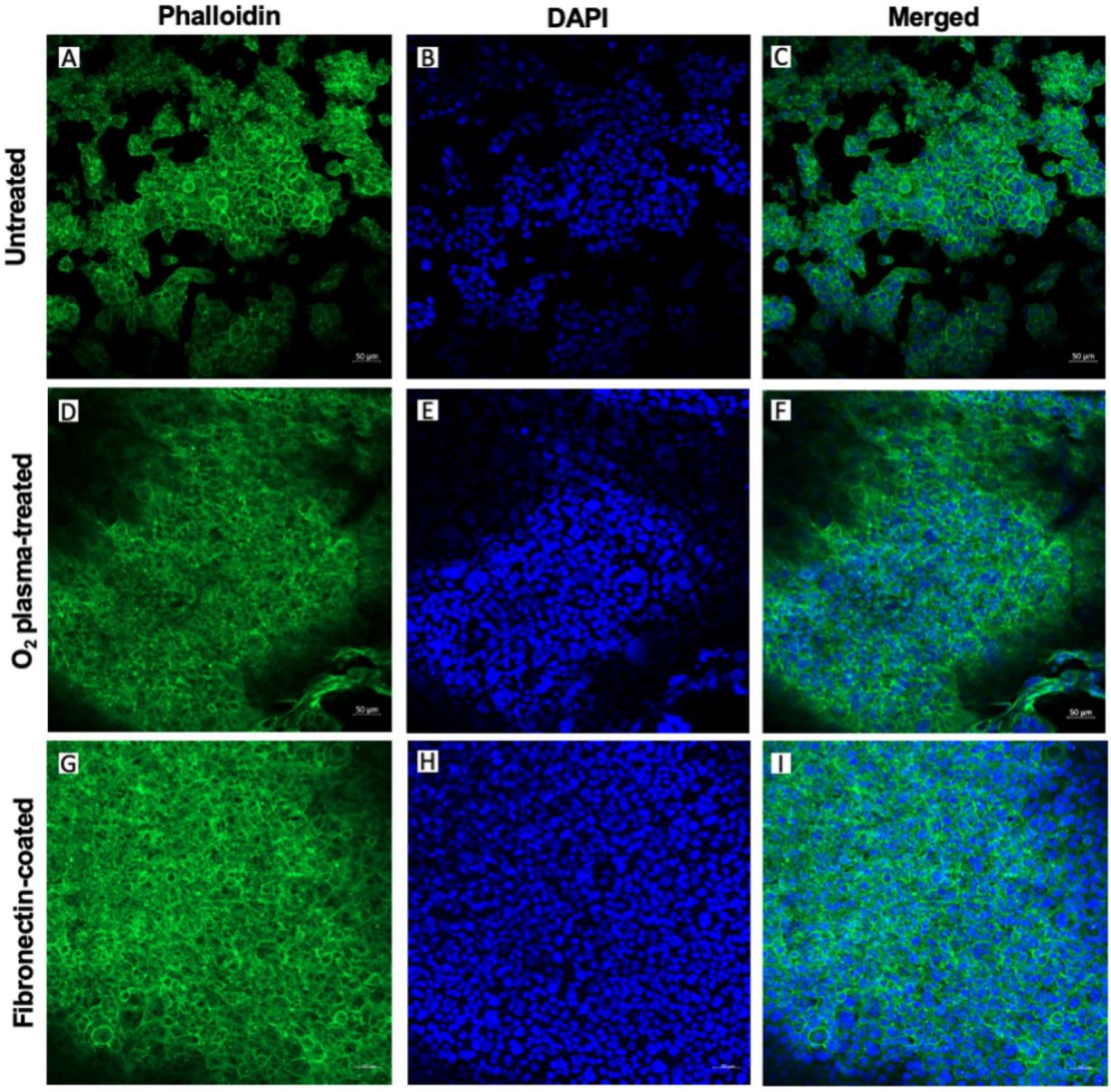

Fig. 5. The CLSM images show TR146 cells seeded on untreated (**A**–**C**), oxygen plasma–treated (**D**–**F**), and fibronectin-coated (**G**–**I**) nanofibrous 12% PLA meshes. Actin filaments were stained with phalloidin (green) on day 2, and cell nuclei were counterstained with DAPI (blue). Scale bar: 50 µm.

and larger pore dimensions. The reduced viscosity of the 10% PLA solution resulted in fibers with elongated beads and a wide range of diameters, whereas the 12% formulation yielded uniformly sized fibers with minimal defects. Although the 10% PLA produced a lower minimum fiber diameter, the irregularity and bead formation diminished the effective surface area for cell anchorage[19,20]. These results support earlier findings that nanofibrous scaffolds offer increased binding sites and surface area for cell attachment compared to microfiber structures.

In more detailed observation, it was found that fibers produced from the 12% PLA formulation demonstrated a more consistent diameter distribution and a lower average diameter compared to those from the 10% PLA formulation. Although the 10% PLA fibers achieved a smaller minimum diameter (approximately 202 nm) compared to the 12% PLA fibers (around 343 nm), the 10% formulation exhibited a broader size distribution due to bead formation. This bead formation not only reduces the effective surface area available for cell attachment but also leads to nonuniform cell growth and clustering, as observed in our 10% PLA samples. Previous studies have shown that the presence of beads in nanofibrous scaffolds is correlated with diminished cell attachment and proliferation[19]. Additionally, the beads may compromise the mechanical flexibility of the fibers, requiring cells to exert more force to attach and spread uniformly on the mesh[19,20].

Pore architecture is critical for controlling cellular behaviour on electrospun scaffolds. The aims of this study was to develop a dense nanofibrous mesh that promotes cell anchorage on its surface while preventing undesirable cell infiltration at the same time, thereby fostering effective cell-cell interactions to form a selective

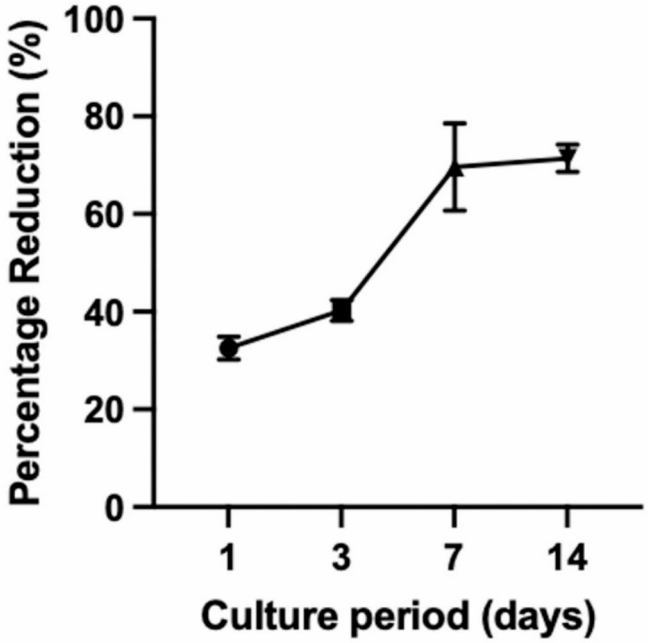

Fig. 6. Increased cellular proliferation over 14 days on fibronectin-coated PLA nanofibrous mesh was observed with PrestoBlue assay. Measurements were performed in triplicate.

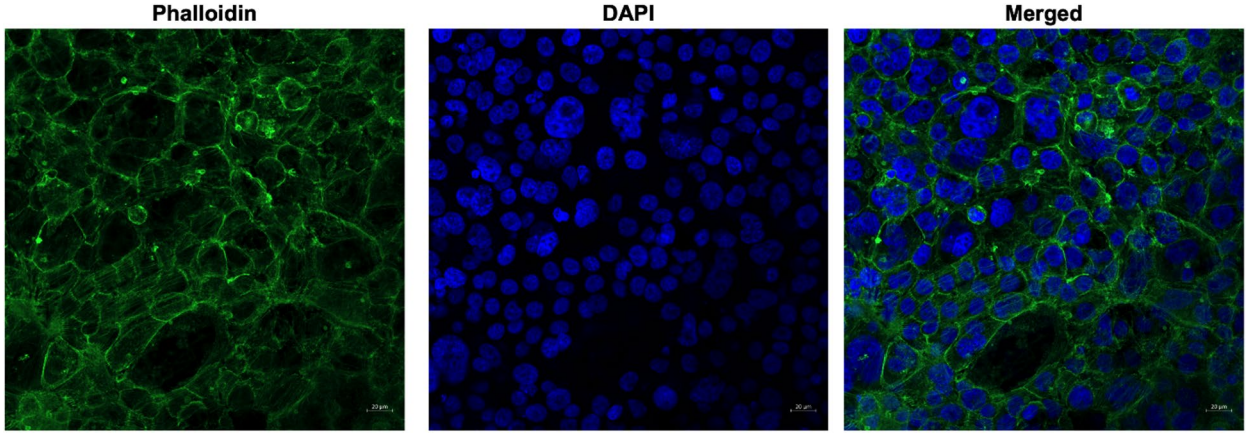

Fig. 7. The CLSM images show TR146 cells seeded on nanofibrous 12% PLA meshes. Actin filaments were stained with phalloidin (green) on day 2, and cell nuclei were counterstained with DAPI (blue). Scale bar: 50 µm.

permeability barrier that mimics the basement membrane[21]. This objective was addressed by engineering an electrospun scaffold with a high fiber density and minimal pore size[22]. Comparative analysis of meshes prepared from 10% to 12% PLA solutions revealed that the 12% formulation offers more favourable pore characteristics for cell adhesion, exhibiting both a lower overall pore area and smaller average pore dimensions. In contrast, confocal imaging of the 10% PLA meshes indicated reduced cell density and potential cell penetration due to higher porosity. Conversely, the 12% PLA scaffolds supported extensive epithelial cell attachment and lateral spreading, resulting in a more uniform cell layer. These observations strongly suggest that the 12% PLA scaffold is better suited for constructing in vitro models of the oral epithelial barrier and was therefore selected for further investigations.

The 12% PLA scaffolds possess excellent cell anchorage properties that can be further enhanced by optimizing their surface characteristics. Since PLA is inherently hydrophobic, its unmodified form may impede cell adhesion[23]. To better replicate the extracellular matrix (ECM) and improve cellular interactions, surface functionalization was performed on the 12% PLA meshes. Wettability assessments on untreated samples and those subjected to O_2 plasma treatment or fibronectin coating were performed.

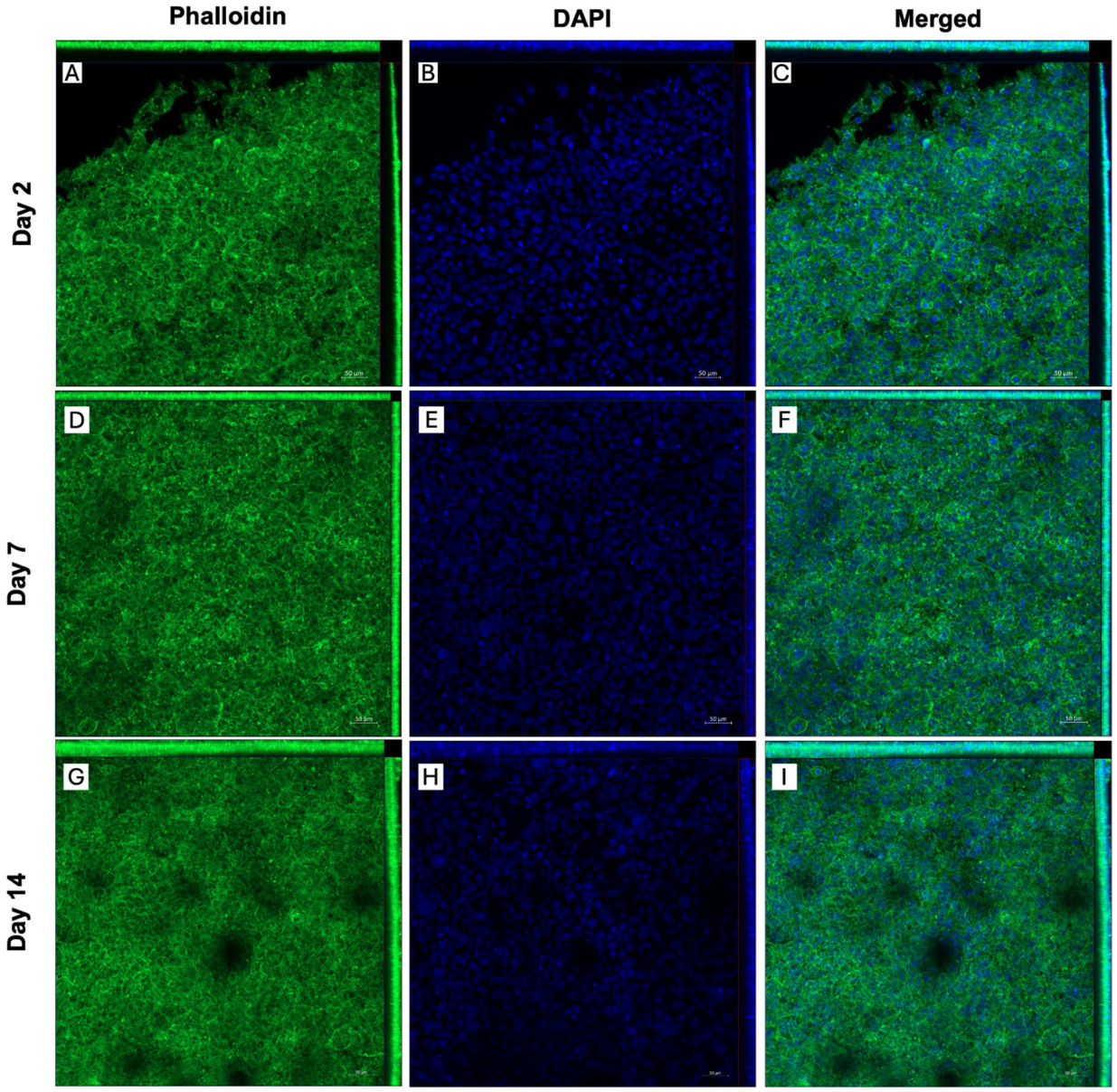

Fig. 8. Z-stack images of TR146 cells seeded on nanofibrous PLA, stained with phalloidin (green) on day 2 (**A**–**C**) and day 7 (**D**–**F**), with nuclei counterstained using DAPI (blue). Images were captured at 1-µm intervals (scale bar: 50 µm). An increase in epithelial cell layering over time is evident from the Z-plane images.

Although O_2 plasma treatment yielded only a slight reduction in hydrophobicity, it nonetheless improved cell attachment and spreading. In contrast, fibronectin coating significantly decreased the surface contact angle; however, the resulting wettability remained outside the theoretically optimal hydrophobicity range for cell attachment (40–70°)[24]. Despite this, confocal microscopy of fibronectin-coated meshes showed superior and more uniform cell distribution compared to unmodified and O_2 plasma-treated samples (Fig. 5). This enhancement is likely due to specific interactions between cell membrane receptors and fibronectin, an essential adhesion protein that facilitates the formation of an ECM-like network on the scaffold[25]. Additionally, the consistent nanoscale fiber structure of the 12% PLA meshes increases the available surface area for protein adsorption, thus expanding the sites for focal adhesion formation and promoting robust cellular integration.

Examination of actin cytoskeletal organization revealed robust cell–material interactions on 12% fibronectin-coated scaffolds. At day 2, epithelial cells exhibited pronounced F-actin accumulation at their periphery, while by day 7, well-developed contractile actin fibers spanned the cell body, signifying stress fiber formation and mature focal adhesion. Such extensive actin remodelling is a recognized marker of strong cell adhesion and effective substrate interaction[26]. Moreover, the presence of lamellipodia at day 7 (Fig. 7A) further indicated the cells' ability to sense and adapt to the nanostructured environment of the scaffold. These findings confirm that the fibronectin-treated electrospun PLA mesh successfully mimics the extracellular matrix, thereby providing a conducive topographical and biochemical landscape for optimal cell attachment and mechanotransduction.

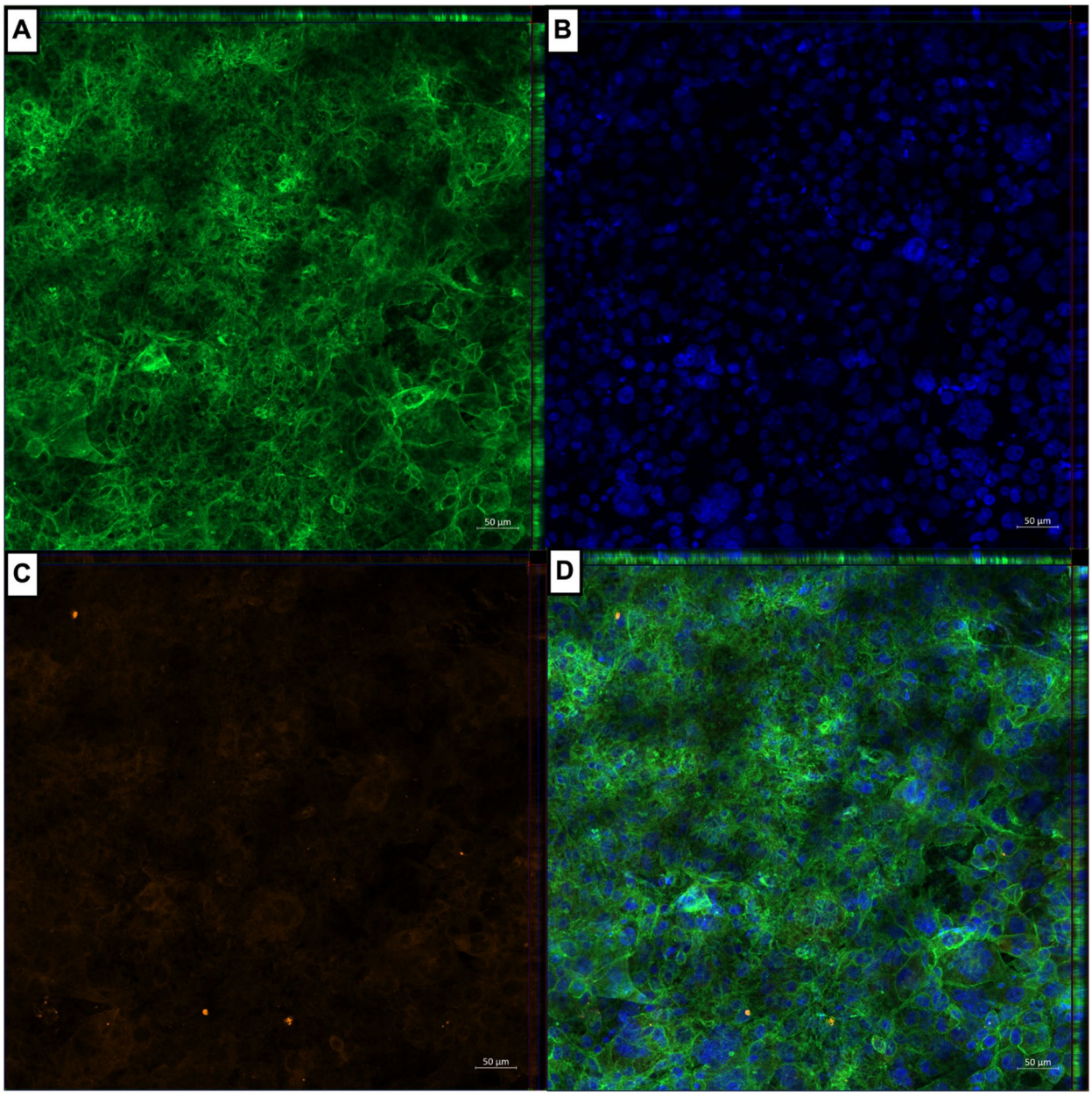

Fig. 9. Tight junction characterization of TR146 cells cultured on the nanofibrous 12% PLA meshes. Actin filaments were stained with phalloidin (green) on day 14 (**A**), and cell nuclei were blue counterstained with DAPI (**B**). Immunofluorescence staining for ZO-1 expression was weak and discontinuous, without clear junctional localization (**C**). Scale bar: 50 µm.

Cell viability and proliferation on the PLA scaffolds were evaluated using both MTS and PrestoBlue assays, applied to cultures with indirect and direct cell seeding. The electrospun PLA exhibited excellent biocompatibility, fostering substantial cell growth and metabolic activity with minimal cytotoxicity from residual solvents. Over a 14-day period, both assays registered rising absorbance levels, indicating sustained proliferation and heightened metabolic function. PrestoBlue analysis further revealed a progressive increase in cell number, culminating in a 2.2-fold rise within 14 days, demonstrating that the scaffold effectively supports cellular expansion.

In comparison to previous studies reporting high viability of Caco-2 cells on PLA fibers for colorectal adenocarcinoma modelling[27] and a trend of increased proliferation in rat aortic smooth muscle cells on PLA fibers until confluency was reached, with a subsequent decline by day 14[28], the findings on this study present a different pattern. The TR146 cells on the PLA mesh continued to proliferate steadily beyond confluency by forming multilayered structures reminiscent of the stratified epithelium found in oral mucosa[29]. Compared with conventional commercial membranes used for TR146 cell seeding, electrospun PLA meshes provide enhanced control over cellular micro-architecture and allow greater customization of scaffold design. These results emphasized the scaffold's capacity to provide a conducive environment for sustained cell growth and

stratification, essential for developing reliable in vitro tissue models for trans-epithelial delivery studies and translational studies.

Oral epithelial cells naturally organize into stratified layers that serve as protective barriers against environmental challenges[29]. This study sought to induce multilayer formation to engineer an effective tissue barrier. It was observed that the electrospun PLA scaffold promotes the development of surface cell layers while preventing unwanted cell penetration into the matrix. Layer formation was consistently evident throughout the culture period, with nuclei-based quantification from confocal z-stack images revealing approximately 2–3 distinct layers on days 2 and 7 (Fig. 8A–F). This steady layering likely reflects a preference for lateral expansion on the scaffold, allowing cells to reach confluence on the surface before vertical stacking occurs, an observation corroborated by significant increases in metabolic activity detected by PrestoBlue assays between days 3 and 7 (Fig. 6B).

Additionally, consistent with findings by Jacobsen and co-workers[30], TR146 cells typically achieve confluence within 9–12 days on standard tissue culture inserts. In this experiments, the multilayered structure further developed by day 14, with a notable increase in thickness indicating around three layers. Previous reports have identified 4–8 layers after 30 days[30] and noted that airlift cultures yield multilayering, whereas submerged conditions usually result in a monolayer[31]. These results highlight the potential of the electrospun PLA mesh as a novel scaffold that fosters favourable cell behaviour. Future investigations should extend the culture duration and explore intercellular junction formation, which is essential for assessing permeability and barrier integrity.

A key strength of this study is the successful development of a tissue-engineered oral mucosal barrier model using PLA electrospun nanofibers that support epithelial cell attachment, viability, and stratification. The nanofibrous architecture closely mimics the native extracellular matrix of the oral mucosa, providing a biologically relevant microenvironment that promotes organized epithelial growth. Compared with conventional flat membrane systems, this three-dimensional scaffold more accurately reflects the structural features of the oral epithelial barrier.

The study also provides comprehensive physicochemical and biological characterization of the scaffold–cell construct, including morphological assessment and cytocompatibility evaluation. These parameters represent essential prerequisites for barrier formation and establish a robust foundation for subsequent trans-epithelial transport and drug delivery studies. The translational applicability of this model is further supported by its application in a separate study on nanoparticle permeability, which has been submitted as an independent manuscript.

Despite these strengths, certain aspects of the model warrant further refinement. Functional barrier integrity assessments, such as transepithelial electrical resistance (TEER) measurements or standardized permeability assays using molecular tracers, were beyond the scope of this work, as the study focused on model development and structural validation rather than functional transport analysis.

Although multilayered epithelial growth was observed on the PLA electrospun nanofibers, further optimization and characterization of epithelial differentiation and junctional markers is needed to clarify the maturation status of the construct. The epithelial barrier characteristics found in this study (Fig. 9) may also be influenced by the inherently leaky phenotype of TR146-derived cells, related to their carcinoma origin and relatively low tight junction protein expression. Accordingly, future studies should incorporate analyses of oral epithelial cytokeratin subtypes and tight junction proteins, as well as long-term assessments of epithelial viability, scaffold degradation, and maintenance of epithelial architecture under extended culture conditions, to further validate the model's suitability for tissue engineering applications.

Furthermore, the current model incorporates a single epithelial cell type and does not yet include additional cellular components of the oral mucosa, such as fibroblasts or immune cells, which may influence barrier function and inflammatory responsiveness. Future integration of multicellular co-culture systems, together with quantitative functional assays, is expected to further enhance the physiological relevance and translational utility of the model.

Conclusions

In this study, an in vitro model of oral epithelium was constructed using electrospun PLA scaffolds. Of the formulations evaluated, the 12% PLA meshes demonstrated a clear advantage, featuring a uniform fiber architecture and reduced pore sizes that significantly enhanced cellular adhesion and proliferation. Further surface modification with fibronectin markedly improved cell attachment and promoted extensive spreading, resulting in dynamic multilayer formation. These findings highlight the promise of fibronectin-coated 12% PLA scaffolds as effective platforms for engineering tissue barriers. Future work should focus on prolonged culture durations and detailed permeability assessments to fully exploit their potential in biomedical applications.

Data availability

The datasets generated and/or analyzed to support the findings of the current study are available from the corresponding author upon reasonable request.

Received: 10 December 2025; Accepted: 24 February 2026
Published online: 01 April 2026

References

1. Jain, N., Dutt, U., Radenkov, I. & Jain, S. WHO's global oral health status report 2022: Actions, discussion and implementation. *Oral Dis.* **30** (2), 73–79 (2024).
2. Mrsny, R. J. Lessons from nature: Pathogen-Mimetic systems for mucosal Nano-medicines. *Adv. Drug Deliv Rev.* **61** (2), 172–192 (2009).

3. Macedo, A. S. et al. Novel and revisited approaches in nanoparticle systems for buccal drug delivery. *J. Controlled Release*. **320**, 125–141 (2020).
4. Şenel, S. An overview of physical, microbiological and immune barriers of oral mucosa. *Int. J. Mol. Sci.* ;**22**(15). (2021).
5. Chen, J., Ahmad, R., Li, W., Swain, M. & Li, Q. Biomechanics of oral mucosa. *J. R Soc. Interface* ;**12**(109). (2015).
6. Boegh, M. & Nielsen, H. M. Mucus as a barrier to drug delivery - Understanding and mimicking the barrier properties. *Basic. Clin. Pharmacol. Toxicol.* **116** (3), 179–186 (2015).
7. Patel, V. F., Liu, F. & Brown, M. B. Advances in oral transmucosal drug delivery. *J. Controlled Release*. **153** (2), 106–116 (2011).
8. Samiei, M. et al. Cell junctions and oral health. *EXCLI J.* **18**, 317–330 (2019).
9. Bierbaumer, L., Schwarze, U. Y., Gruber, R. & Neuhaus, W. Cell culture models of oral mucosal barriers: A review with a focus on applications, culture conditions and barrier properties. *Tissue Barriers* ;**6**(3). (2018).
10. Ali, A., Wahlgren, M., Pedersen, L. & Engblom, J. Will a water gradient in oral mucosa affect transbuccal drug absorption? *J. Drug Deliv Sci. Technol.* **48**, 338–345 (2018).
11. Mazzinelli, E. et al. Oral Mucosa Models to Evaluate Drug Permeability. *Pharmaceutics* ;**15**(5). (2023).
12. Costa, C. M., de Carvalho, N. M., de Oliveira, D. L. & Madureira, A. R. A Critical Review on In Vitro and Ex Vivo Models of the Intestinal Epithelium of Humans and Monogastric Animals. *Gastrointest. Disorders*. **6** (1), 337–358 (2024).
13. Anjum, S. et al. Electrospun Biomimetic Nanofibrous Scaffolds: A Promising Prospect for Bone Tissue Engineering and Regenerative Medicine. *Int. J. Mol. Sci.* ;**23**(16). (2022).
14. Wang, X., Ding, B. & Li, B. Biomimetic electrospun nanofibrous structures for tissue engineering. *Mater. Today*. **16** (6), 229–241 (2013).
15. Muniyandi, P. et al. ECM mimetic electrospun porous poly (l-lactic acid) (PLLA) scaffolds as potential substrates for cardiac tissue engineering. *Polym. (Basel)* ;**12**(2). (2020).
16. Aazmi, A. et al. Biofabrication methods for reconstructing extracellular matrix mimetics. *Bioact Mater.* **31**, 475–496 (2024).
17. Zulkifli, M. Z. A., Nordin, D., Shaari, N. & Kamarudin, S. K. Overview of Electrospinning for Tissue Engineering Applications. *Polym. (Basel)* ;**15**(11). (2023).
18. Ferraris, S. et al. Topographical and biomechanical guidance of electrospun fibers for biomedical applications. *Polym. (Basel)*. **12** (12), 1–32 (2020).
19. Chen, M., Patra, P. K., Warner, S. B. & Bhowmick, S. Role of fiber diameter in adhesion and proliferation of NIH 3T3 fibroblast on electrospun polycaprolactone scaffolds. *Tissue Eng.* **13** (3), 579–587 (2007).
20. Chen, M., Patra, P. K., Lovett, M. L., Kaplan, D. L. & Bhowmick, S. Role of electrospun fibre diameter and corresponding specific surface area (SSA) on cell attachment. *J. Tissue Eng. Regen Med.* **3** (4), 269–279 (2009).
21. Jain, P., Rauer, S. B., Möller, M. & Singh, S. Mimicking the Natural Basement Membrane for Advanced Tissue Engineering. *Biomacromolecules* **23** (8), 3081–3103 (2022).
22. Liverani, L., Killian, M. S. & Boccaccini, A. R. Fibronectin functionalized electrospun fibers by using benign solvents: Best way to achieve effective functionalization. Front Bioeng Biotechnol. ;7(APR). (2019).
23. Castañeda-Rodríguez, S. et al. Recent advances in modified poly (lactic acid) as tissue engineering materials. *J. Biol. Eng.* ;**17**(1). (2023).
24. Al-Azzam, N. & Alazzam, A. Micropatterning of cells via adjusting surface wettability using plasma treatment and graphene oxide deposition. *PLoS One* ;**17** (2022). (6 June).
25. Parisi, L. et al. A glance on the role of fibronectin in controlling cell response at biomaterial interface. *Japanese Dent. Sci. Rev.* **56** (1), 50–55 (2020).
26. Jain, P., Rimal, R., Möller, M. & Singh, S. Topographical influence of electrospun basement membrane mimics on formation of cellular monolayer. *Sci. Rep.* ;**13**(1). (2023).
27. Ricci, C. et al. Assessment of Electrospun Poly(ε-caprolactone) and Poly(lactic acid) Fiber Scaffolds to Generate 3D In Vitro Models of Colorectal Adenocarcinoma: A Preliminary Study †. *Int. J. Mol. Sci.* ;**24**(11). (2023).
28. Barrientos, I. J. H., MacKenzie, G. R., Wilson, C. G., Lamprou, D. A. & Coats, P. Biological performance of electrospun polymer fibres. *Materials* ;**12**(3). (2019).
29. Groeger, S. & Meyle, J. Oral mucosal epithelial cells. *Front. Immunol.* **10** (FEB), 1–22 (2019).
30. Papers, R., Jacobsen, J., Van Deurs, B., Pedersen, M. & Rassing, M. R. TR146 cells grown on filters as a model for human buccal epithelium: I. Morphology, growth, barrier properties, and permeability. *Int. J. Pharm.* **125**, 165–184 (1995).
31. Lin, G. C. et al. Optimization of an oral mucosa in vitro model based on cell line TR146. *Tissue Barriers*. **8** (2), 1748459 (2020).

Acknowledgements

This study forms part of the doctoral thesis of Andari Sarasati. The authors acknowledge the Ministry of Education, Research, and Technology of the Republic of Indonesia and RISPRO–LPDP (Indonesia Endowment Fund) for supporting the "MicroLung Project" (PRPB), which facilitates collaboration between UGM and ACU under contract number 014/E5/PG.02.00/PRPB and enables the use of research facilities at the ACU Biomaterials Centre. The authors also extend their gratitude to the Ministry of Education, Research, and Technology for additional grant support analysis in Indonesia. The authors thank the Scientific Imaging Centre (SIC), Bandung Institute of Technology, for providing access to the CLSM facility. This study received ethical approval from the Research Ethics Committee, Faculty of Dentistry, Universitas Gadjah Mada, under approval number 142/KE/FKG-UGM/EC/2022. This publication is funded by the Indonesian Endowment Fund for Education (LPDP) on behalf of the Indonesian Ministry of Higher Education, Science and Technology and managed under the EQUITY Program (Contract Number: 4301/B3/DT.03.08/2025 and 10107/UN1.P/Dit-Keu/HK.08.00/2025).

Author contributions

AS : Methodology; Investigation; Formal analysis; Visualization; Supervision; Validation; Writing – substantial part of original draft DYU : Methodology; Formal analysis; Supervision; Validation; Writing – review, editing. HKE : Methodology; Formal analysis; Supervision; Validation; Writing – review, editing. HWI : Formal analysis; Supervision; Validation; IDA : Conceptualization; Methodology; Resources; Formal analysis; Validation; Writing – original draft, review, editing. RAH : Methodology; Formal analysis; Supervision; Validation. NSO : Investigation; Formal analysis. VAH : Conceptualization; Methodology; Resources; Formal analysis; Validation; Writing – review, editing.

Funding

The analytical work performed at UGM was supported by the Ministry of Education, Research, and Technology of the Republic of Indonesia under contract number 018/E5/PG.02.00.PL/2023, with supporting document

numbers: 2182/UN1/DITLIT/Dit-Lit/PT.01.03/2023, 165.19/E4.4/KU/2023 and 4696/E4/DT.04.02/2023. The collaborative work conducted in this study, including the provision of TR146 cells, was supported by the "MicroLung Project" (PRPB) under contract number 014/E5/PG.02.00/PRPB, which also enabled access to research facilities at the ACU Biomaterials Centre.

Declarations

Competing interests

The authors declare no competing interests.

Additional information

Supplementary Information The online version contains supplementary material available at https://doi.org/10.1038/s41598-026-42105-x.

Correspondence and requests for materials should be addressed to I.D.A.

Reprints and permissions information is available at www.nature.com/reprints.

Publisher's note Springer Nature remains neutral with regard to jurisdictional claims in published maps and institutional affiliations.

Open Access This article is licensed under a Creative Commons Attribution-NonCommercial-NoDerivatives 4.0 International License, which permits any non-commercial use, sharing, distribution and reproduction in any medium or format, as long as you give appropriate credit to the original author(s) and the source, provide a link to the Creative Commons licence, and indicate if you modified the licensed material. You do not have permission under this licence to share adapted material derived from this article or parts of it. The images or other third party material in this article are included in the article's Creative Commons licence, unless indicated otherwise in a credit line to the material. If material is not included in the article's Creative Commons licence and your intended use is not permitted by statutory regulation or exceeds the permitted use, you will need to obtain permission directly from the copyright holder. To view a copy of this licence, visit http://creativecommons.org/licenses/by-nc-nd/4.0/.

© The Author(s) 2026